INSTRUCTIONAL LABORATORIES AND DEMONSTRATIONS | APRIL 01 2026

Swept-source and spectral-domain optical coherence tomography—Educational setups for the undergraduate lab

Keerthanan Ulaganathan ; Kai Pieper ; Max Althön ; Antje Bergmann ; Carsten Rockstuhl ; Jens Küchenmeister

Am. J. Phys. 94, 321–330 (2026)
https://doi.org/10.1119/5.0300824

INSTRUCTIONAL LABORATORIES AND DEMONSTRATIONS

John Essick, *Editor*
Department of Physics, Reed College, Portland, OR 97202

Articles in this section deal with new ideas and techniques for instructional laboratory experiments, for demonstrations, and for equipment that can be used in either. Although these facets of instruction also appear in regular articles, this section is for papers that primarily focus on equipment, materials, and how they are used in instruction. Manuscripts should be submitted using the web-based system that can be accessed via the American Journal of Physics home page, ajp.aapt.org, and will be forwarded to the IL&D editor for consideration.

Swept-source and spectral-domain optical coherence tomography—Educational setups for the undergraduate lab

Keerthanan Ulaganathan,[1,a)] Kai Pieper,[2,b)] Max Althön,[1,c)] Antje Bergmann,[3,d)] Carsten Rockstuhl,[3,4,e)] and Jens Küchenmeister[1,f)]
[1]*Thorlabs GmbH, Münchner Weg 1, 85232 Bergkirchen, Germany*
[2]*Markgraf-Ludwig-Gymnasium, Hardstr. 2, 76530 Baden-Baden, Germany*
[3]*Institute of Theoretical Solid State Physics, Karlsruhe Institute of Technology, Wolfgang-Gaede-Str. 1, 76131 Karlsruhe, Germany*
[4]*Institute of Nanotechnology, Karlsruhe Institute of Technology, P.O. Box 3640, 76021 Karlsruhe, Germany*

(Received 4 September 2025; accepted 16 January 2026)

Optical coherence tomography (OCT) has become increasingly important in fundamental research, medical diagnostics, material characterization, and industrial process monitoring. OCT measures the depth-dependent reflectivity of a sample with micrometer-scale resolution by analyzing the interference between light reflected from the sample and a reference arm. Despite its widespread application, OCT remains underrepresented in undergraduate curricula due to the complexity and cost of commercial systems. Our contribution presents educational implementations of the two most widely used OCT modalities: swept-source OCT and spectral-domain OCT. In our swept-source setup, a grating monochromator is used as a tunable light source, providing a clear and cost-effective realization of wavelength sweeping. For our spectral-domain setup, we developed a compact, self-built two-dimensional spectrometer enabling efficient spectral acquisition. Both systems are capable of producing three-dimensional representations of the internal sample structure. Designed with open architecture and minimal complexity, these setups prioritize visibility of core principles, making them well-suited for hands-on learning in undergraduate laboratory environments.
https://doi.org/10.1119/5.0300824

I. INTRODUCTION

Optical coherence tomography (OCT) is an interferometric imaging technique that produces depth-resolved, three-dimensional images of samples by detecting light reflected from optical interfaces, i.e., regions where the refractive index changes. OCT has found widespread use across medical and industrial fields. In particular, it has become the gold standard in ophthalmology.[1] Other medical fields applying OCT include cardiology[2] and gastroenterology.[3] Further applications range from quality control in contact lens manufacturing[4] to the analysis of biofilms[5] and the non-destructive examination of artwork.[6]

Despite its widespread use, the educational potential of OCT remains underexplored. OCT provides a rich context for connecting abstract concepts, such as coherence, interferometry, and spectral analysis, to practical measurements, making it a powerful tool for advanced undergraduate instruction. From a pedagogical perspective, OCT enables students to revisit interferometry principles, measure wavelengths, observe white-light interference, and explore how the coherence length of a light source determines axial resolution. These topics reinforce core optics concepts in an application-driven setting.

While time-domain OCT has been successfully implemented in teaching,[7] Fourier-domain OCT, comprising spectral-domain and swept-source approaches, offers additional learning opportunities and represents the current state-of-the-art. Fourier-domain OCT introduces Fourier analysis in a practical context and demonstrates the relationship between modulation frequency on the spectrum and optical path difference. It also allows exploration of sampling effects and sensitivity roll-off, concepts that generalize to signal processing. A low-cost spectral-domain OCT device has been reported,[8] but its black-box design hinders understanding of the underlying mechanisms.

In this work, we present an open, modular OCT setup for undergraduate laboratories that includes both spectral-domain

and swept-source configurations and can be combined with a previously published time-domain OCT setup.[7] The spectral-domain implementation employs a self-built camera-based spectrometer, introducing students to spectroscopy principles through construction and use of the spectrometer. The swept-source implementation uses a self-built grating monochromator for tunable illumination, which allows verification of the generalized grating equation by measuring wavelength-dependent diffraction angles. In both implementations, 3D data can be collected, and the spectral-domain setup even enables real-time cross-sectional imaging of the sample at a 50 Hz acquisition rate. In addition to understanding the physically rich imaging mechanism, the setups can also be used for other investigations, such as refractive index measurements and light source characterization. This experiment is intended for the final stage of undergraduate studies, when students have the necessary theoretical background. The degree of experimental difficulty can be adjusted by the extent to which the instructor pre-builds and pre-aligns the setup. At this stage, the setup allows instructors to tie multiple topics together in a comprehensive, hands-on experience.

The paper is structured as follows: After giving an overview of OCT in Sec. II, the necessary theory is presented in Sec. III. In Sec. IV, the design, setup, and data processing of the swept-source setup are described, followed by the same for the spectral-domain setup in Sec. V. The measured data for the different setups are then compared in Sec. VI. We conclude on this work in Sec. VII.

II. OVERVIEW OF OPTICAL COHERENCE TOMOGRAPHY

While there are many different OCT modalities,[9–11] three main approaches can be distinguished. In time-domain OCT,[7] a broadband, and therefore low-coherence, light source illuminates a sample in one arm of a Michelson interferometer, while a reference mirror in the other arm scans mechanically. Interference occurs only when the optical path lengths of the sample and reference arms match within the coherence length of the source. Thus, each reflective interface within the sample produces a localized interferogram as the mirror scans, allowing depth profiles to be reconstructed and assembled into a three-dimensional image.

Although time-domain OCT was the first implementation of the technique, it has largely been replaced by two Fourier-domain methods: spectral-domain and swept-source OCT. Both are based on the same physical principle:[12] Depth-resolved information is obtained by analyzing the spectral interference pattern produced when light reflected from different depths within the sample interferes with light from a fixed reference arm. The modulation arises from the different interference conditions of the wavelength components. Each reflector's depth corresponds to a unique modulation frequency on the spectrum. Figure 1(c) shows an example of a modulated spectrum for the simplest case of a single reflector. By capturing the entire modulated spectrum, a Fourier transform can be used to analyze the modulation frequencies, which yields the entire depth profile in a single measurement, eliminating the need for mechanical scanning of the reference mirror that is required in time-domain OCT.

Spectral-domain OCT [Fig. 1(a)] and swept-source OCT [Fig. 1(b)] differ in how the modulated spectrum is recorded. In spectral-domain OCT, a broadband light source illuminates the interferometer and a spectrometer is used to record the modulated spectrum corresponding to the depth profile at a single lateral position of the sample (A-scan). The sample at that lateral position can be idealized as a series of discrete reflecting interfaces. In swept-source OCT, the sample is illuminated by a source with a narrow linewidth and tunable wavelength. The resulting intensity at the interferometer output is recorded for each wavelength in the tuning range to acquire the modulated spectrum over time. For both methods, a beam scanner is typically used to illuminate a transverse line of the sample to capture a 2D image (B-scan) or an area of the sample to capture a full 3D image.

III. THEORY

First, consider a Michelson interferometer [see, e.g., Fig. 1(b)] with a reference mirror at a distance z_R to the beam splitter and a single reflector in the sample arm at a distance z_1 to the beam splitter. The reflectivity from each interface is R_R and R_1, respectively. The interferometer is illuminated by a light source with power spectrum $S(k)$, where $k = 2\pi/\lambda$ represents the wave number and λ denotes the wavelength. The intensity at the output of the interferometer is given by[12]

$$I(k) = \frac{1}{4}S(k)(R_R + R_1) + \frac{1}{2}S(k)\sqrt{R_R R_1}\cos\big(2k(z_1 - z_R)\big). \tag{1}$$

The first term in Eq. (1) does not depend on the distances between the interfaces. It is given by the light source's spectrum and the reflectivity. Therefore, it is constant and often referred to as the "DC term." The second term contains the desired signal, and is called the "cross-correlation term." The cross-correlation term describes the interference between light reflected from the sample interface with light reflected from the reference. The oscillation frequency of the cosine is proportional to the distance between the sample and reference interfaces relative to the beam splitter. This distinct modulation frequency within the spectrum, see Fig. 1(c), corresponds to the difference in optical path lengths to the interface and reference and can be identified via a Fourier transform of the modulated spectrum. Under the assumption that the reflectivities are constant over the relevant wave number interval, the absolute value of the Fourier transformed signal is proportional to[12]

$$|i(z)| \propto A(z)(R_R + R_1) + 2\sqrt{R_R R_1}[A(z + (z_R - z_1)) + A(z - (z_R - z_1))], \tag{2}$$

where $A(z) = \mathcal{F}[S(k)]$ is the Fourier transform of the power spectrum of the light source. For OCT, $S(k)$ is assumed to be sufficiently broadband and well-behaved such that $A(z)$ is a localized function with a single dominant maximum. The first term of Eq. (2) corresponds to the DC term, while the second term corresponds to the cross-correlation term with two peaks at $\pm(z_R - z_1)$. Because of the symmetry, we can restrict ourselves to one peak, e.g., at positive z-values. Importantly, the width and shape of the peak is determined by the power spectrum $S(k)$. For a broad spectrum, the peak after the Fourier transform becomes narrow and vice versa. This determines the axial resolution, i.e., the resolution in z. More specifically, the axial resolution is based on the coherence length l_c of the light source, which is often approximated by a Gaussian spectrum with a center wavelength λ_0 and full width at half-maximum $\Delta\lambda$,[12]

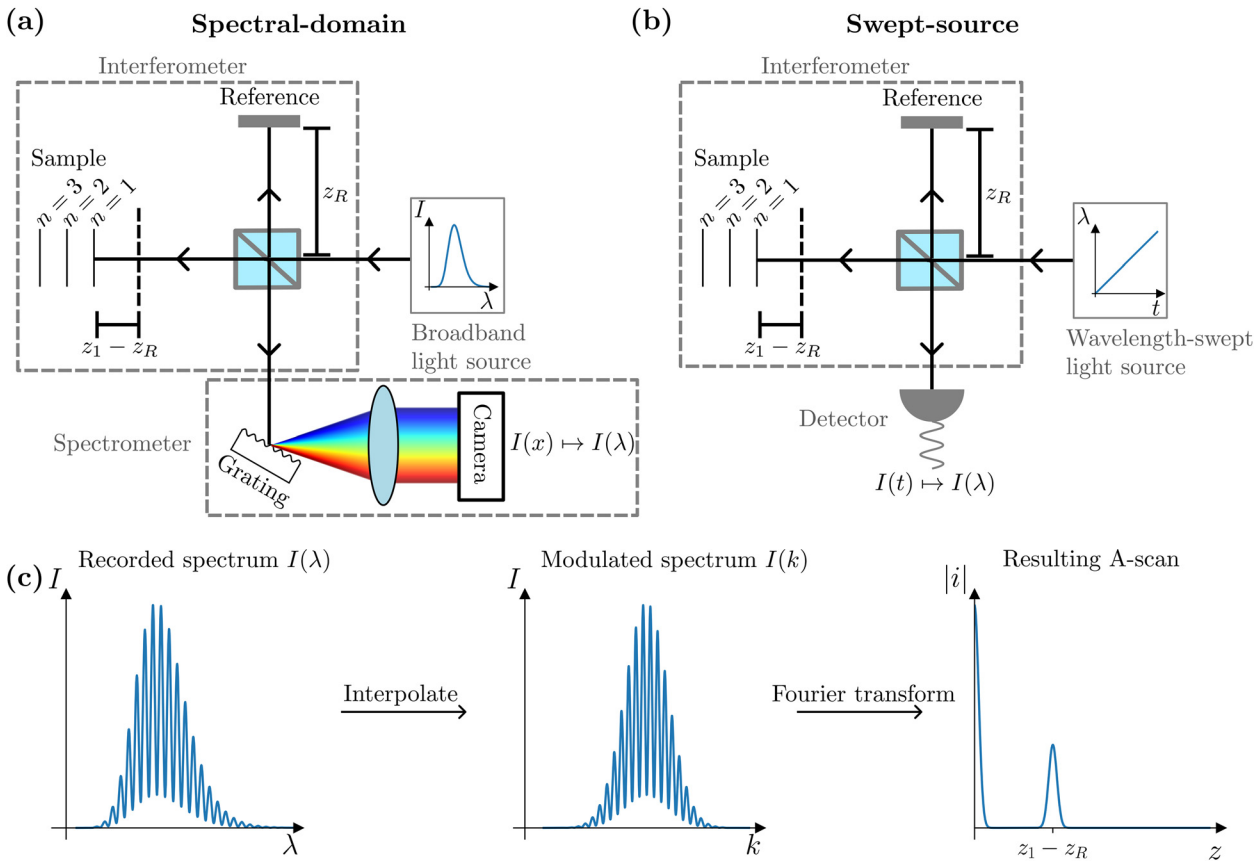

Fig. 1. (Color online) Schematic overview of Fourier-domain OCT. The technique relies on recording a spectrum $I(\lambda)$, where I is the intensity and λ is the wavelength, and depth information arises from spectral interference between the reference and sample arms of an interferometer. Spectral-domain and swept-source are the two main data-taking methods, which differ in the way $I(\lambda)$ is recorded. (a) Spectral-domain: A broadband light source illuminates the interferometer and a spectrometer is placed at the interferometer output. (b) Swept-source: The wavelength of the light source is swept through its range and the intensity at the interferometer output is measured with a photodetector. In (a) and (b), the recorded spectrum $I(\lambda)$ encodes the depth profile of the sample at a single lateral position. The sample at that lateral position can be idealized as a series of discrete reflecting interfaces located at distances z_n. For both methods, a beam scanner is typically used to illuminate a transverse line of the sample to capture a 2D image (B-scan) or an area of the sample to capture a full 3D image. (c) The recorded spectrum $I(\lambda)$ is transformed into $I(k)$, where $k = 2\pi/\lambda$ represents the wave number. We call $I(k)$ the *modulated spectrum*. The modulated spectrum is Fourier transformed to obtain the optical depth structure $|i(z)|$ (A-scan). The modulated spectrum and Fourier transformed result represent a single reflector in the sample arm, where the optical path length to the sample reflector z_1 differs from the optical path length to the reference mirror z_R. The large peak at $z = 0$ comes from the DC component, i.e., the average intensity of the modulated spectrum.

$$l_c \approx \frac{2\ln(2)\lambda_0^2}{\pi\Delta\lambda}. \tag{3}$$

For a general sample, idealized as a set of discrete reflecting interfaces located at distances z_n from the beam splitter, the intensity at the output of the interferometer can be expressed as[12]

$$\begin{aligned} I(k) = {} & \frac{1}{4}\left(S(k)\left(R_R + \sum_{n=1}^{N} R_n\right)\right) \quad \text{“DC Terms”} \\ & + \frac{1}{2}\left(S(k)\sum_{n=1}^{N}\sqrt{R_R R_n}\cos\left(2k(z_R - z_n)\right)\right) \\ & \text{“Cross−correlation Terms”} \\ & + \frac{1}{4}\left(S(k)\sum_{n=1}^{N}\sum_{\substack{m=1 \\ m\neq n}}^{N}\sqrt{R_n R_m}\cos\left(2k(z_n - z_m)\right)\right) \\ & \text{“Auto−correlation Terms”}. \end{aligned} \tag{4}$$

Multiple reflections within the sample are neglected for this expression, as the typical reflectivities are small. For a sample with multiple interfaces, additional terms are obtained, which are called “auto-correlation.” The auto-correlation terms are independent of the reference arm and represent interference between light reflected from different interfaces within the sample. Similar to Eq. (2), after Fourier transformation, there is a peak for each of the cross-correlation terms and each of the auto-correlation terms.

In practice, $I(k)$ is sampled over a wave number range Δk_s in N equidistant points k_j $(j = 1, \ldots, N)$. After a discrete Fourier transform, commonly a fast Fourier transform, the result $|i(z_\ell)|$ is obtained. Because of the symmetry in Eq. (2), $N/2 + 1$ sampled points z_ℓ $(\ell = 0, \ldots, N/2)$ are independent. From the properties of the discrete Fourier transform, it follows that the depth samples are spaced equidistantly by $\delta z = z_{\ell+1} - z_\ell$,

$$\delta z = \frac{1}{2}\frac{2\pi}{\Delta k_s}, \tag{5}$$

where the factor of $1/2$ arises from the double pass within the interferometer arms.

An important limitation of Fourier-domain systems is the spectral resolution with which $I(k)$ can be recorded. Beyond

a certain modulation frequency, the system is no longer able to resolve the modulation, and thus the Fourier transform cannot identify the corresponding path length difference. The signal-to-noise ratio of the result after Fourier transform decreases continuously up to this point, which is called "signal roll-off." The signal-to-noise ratio is halved at the path length difference,[12]

$$z_{6\mathrm{dB}} \approx \frac{\ln(2)\lambda_0^2}{\pi\delta\lambda}. \tag{6}$$

Looking at Eq. (3), we can see that this is directly related to the coherence length of the measured wavelength components. The factor of two difference between Eqs. (3) and (6) comes from the double-pass through the interferometer arms. For spectral-domain OCT, $\delta\lambda$ is determined by the wavelength resolution of the spectrometer, which includes wavelength sampling by the camera. For swept-source OCT, $\delta\lambda$ is mainly determined by the linewidth of the source, provided that the wavelength sampling step size is smaller than the linewidth.

IV. SETUP AND MEASUREMENT—SWEPT-SOURCE OCT

In this section, we explain how we implemented an educational swept-source, how the setup is aligned, and how data acquisition and processing are performed to gain full 3D information of the sample.

A. Experimental realization

A fundamental design goal for this educational setup was to make the wavelength sweep visible to the naked eye. To achieve this, we constructed a grating monochromator designed to operate in combination with a white-light LED. The setup is shown in Fig. 2. A white-light LED with a nearly Gaussian spectrum [see Fig. 7(a)] is focused on an entry slit. A subsequent lens collimates the light, which then illuminates the grating. A lens after the grating focuses the light onto an exit slit. The grating is mounted on a motorized rotation stage. Thereby, the wavelength of the light exiting the second slit can be chosen by the rotation angle of the stage. The narrow-linewidth light exiting the monochromator is collimated by a lens, focused by a cylindrical lens to increase intensity and enters the interferometer. We choose a full-field configuration, which means that a sharp image of the sample is mapped onto the camera sensor via the objective lens and tube lens. This enables lateral assignment of depth information. The swept-source measurement is performed by rotating the grating from one end of the LED's spectrum to the other, while the camera collects images at different wavelengths. Thus, for each pixel of the camera, a spectrum is recorded.

B. Calibration

To relate the angle of the grating to the wavelength exiting the monochromator, we use the generalized grating equation given by

$$m\lambda = d\sin(-\gamma) + d\sin(\theta - \gamma), \tag{7}$$

where the groove spacing of the grating is denoted as d, and the diffraction order m is equal to one in our case. The angle γ is the angle between the incident beam and the grating

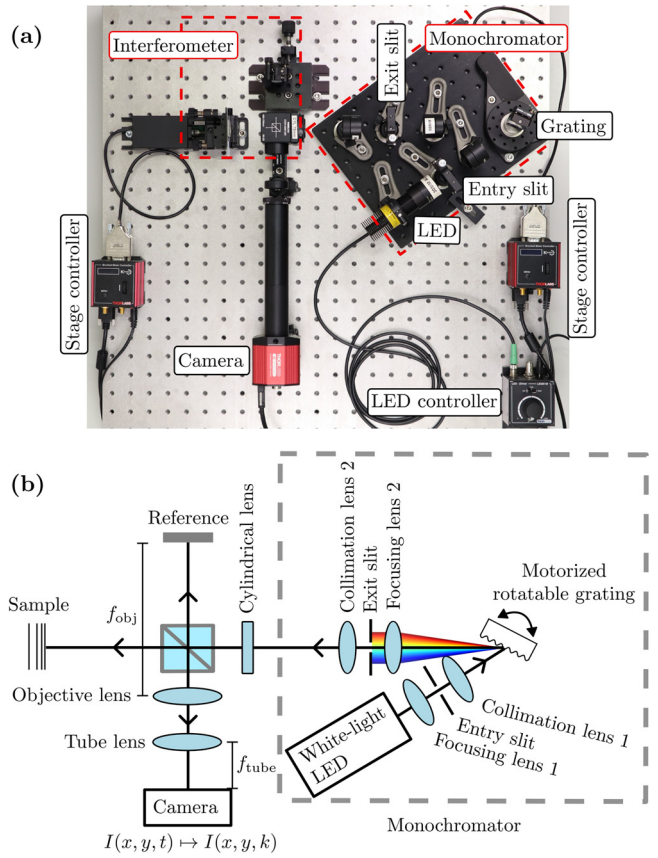

Fig. 2. (Color online) (a) Photograph of the swept-source setup. (b) Schematic of the beam path for the swept-source OCT configuration. Light from the LED is focused through the entry slit, collimated, and illuminates a holographic grating. The dispersed light is collected by a lens, which forms a sharp image of the entry slit on the monochromator's exit slit for each wavelength component. The narrow-linewidth light exiting the monochromator is collimated and then focused by a cylindrical lens before entering the Michelson interferometer. The resulting interference is subsequently detected by the camera, which captures a sharp image of the sample. This image is formed on the camera sensor by the objective and tube lenses, enabling lateral assignment of depth information. The swept-source measurement is performed by rotating the grating, while the camera collects images at different wavelengths.

normal and θ is the diffraction angle. For the monochromator, θ is the angle between the incident beam and the beam that passes through the exit slit. Because the diffraction angle θ remains fixed, the output wavelength is changed by varying the angle γ through rotation of the grating. Figure 3(a) illustrates the definitions of these angles.

To calculate the wavelength that is fed into the interferometer, the angles γ and θ need to be determined. First, the grating is rotated until the zeroth-order beam is directed back through the entry slit. In this configuration, the grating is perpendicular to the light path. This defines the angle $\gamma = 0°$, see Fig. 3(b). The rotation angle γ relative to this position is provided by the stage. To determine θ, the stage is rotated so that the zeroth-order beam is directed into the exit slit, see Fig. 3(c). The grating rotation angle necessary to achieve this is the calibration angle γ_{cal}, see Fig. 3(c). From the calibration angle, the angle between entry and exit slit can be calculated as $\theta = 2 \cdot \gamma_{\mathrm{cal}}$. Using Eq. (7), one can then calculate the wavelength exiting the monochromator for a given angle γ, which can be read out from the rotation stage. Example values for our setup are $\theta = 2 \cdot \gamma_{\mathrm{cal}} = 2 \cdot 18°$, $d = 1/2400\,\mathrm{mm}$, $\gamma_{\mathrm{Start}} = -44.0°$ ($\lambda = 700\,\mathrm{nm}$), and $\gamma_{\mathrm{End}} = -21.1°$ ($\lambda = 500\,\mathrm{nm}$).

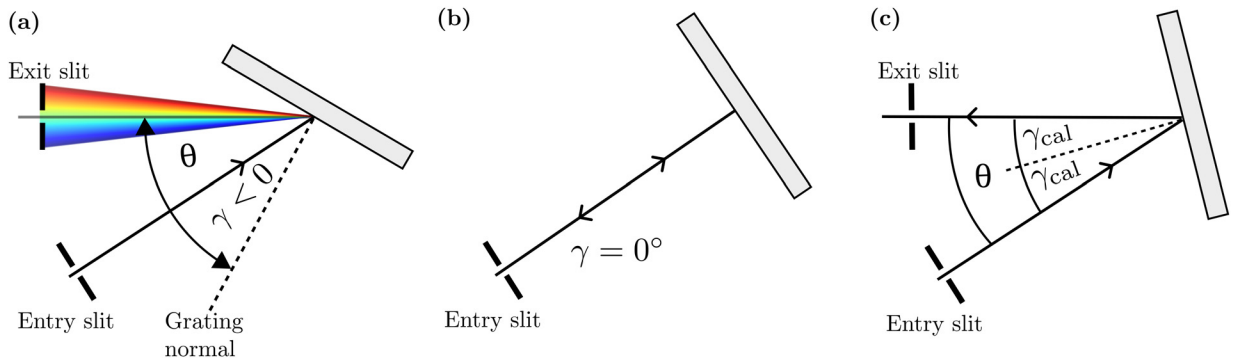

Fig. 3. (Color online) Angle definitions and calibration for the monochromator. (a) The angle γ is between the incoming beam and the grating normal. In the displayed case, it is defined as negative. The swept source is defined by the diffraction angle θ, which is the angle between the beam coming from the entry slit, and the beam that passes through the exit slit. To determine θ, the grating is rotated to the position where the zero-order light is directed back into the entry slit, (b), and the position where the zero-order light is reflected and exits through the second slit, (c). The rotation angle between the two positions is γ_{cal}, with $\theta = 2\gamma_{\text{cal}}$.

C. Data acquisition and processing

Assuming that the stage rotates at a constant angular velocity ω for the measurement duration T and L images are acquired along the way, the rotation results in equidistant angular steps $\delta\gamma = \omega T/L = (\gamma_{\text{End}} - \gamma_{\text{Start}})/L$ between the images. It is advantageous to use a high groove density grating, such as the 2400 lines/mm holographic grating used in this work, because this results in larger angular steps, making the setup less susceptible to fluctuations in stage movement. Following Eq. (7), the wave number for image $j = 1, \ldots, L$ is then given by

$$k_j \approx \frac{2\pi}{d\sin(-\gamma_{\text{Start}} - j\delta\gamma) + d\sin(\theta - \gamma_{\text{Start}} - j\delta\gamma)}. \quad (8)$$

This is an approximation since the stage keeps rotating during the exposure time. Also, this assumes linear motion of the stage in order to provide a constant angular velocity. We have verified that the stage used in the setup provided sufficiently linear motion.

As described above, we employ a full-field geometry in which a sharp image of the sample is formed on the camera. For each camera pixel, the measurement provides a modulated spectrum acquired at equidistant angular steps, see Fig. 4(a). The wave number corresponding to each angle is then calculated according to Eq. (8). Because the grating equation is nonlinear, the wave number spacing between images is nonuniform. To apply a standard fast Fourier transform, the data must be resampled onto an equidistant wave number grid, which is achieved by linear interpolation [Fig. 4(b)]. Applying a Fourier transform to the resampled spectrum then yields the depth information for that pixel.

In a typical lab course, students should be guided through the steps outlined in this section, and instructors should supply the software for data acquisition and processing. Developing such software from scratch would be challenging for students and require skills and time beyond the scope of most instructional laboratory settings. We are happy to share the software we have developed.

D. Performance

The lateral resolution and the field-of-view are determined by the microscope part of the setup, i.e., the objective lens, tube lens, and camera. The microscope in this setup is infinity-corrected with the camera sensor in the focal plane of the tube lens. The optical resolution is primarily determined by the 75 mm objective lens, while the magnification is determined by the 200 mm tube lens. This configuration ensures that the camera's pixel size does not become the limiting factor for lateral resolution. In our testing, we could resolve the lines of group 7 element 3 of a 1951 USAF target, corresponding to a lateral resolution of 6 μm.

The axial resolution is equal to the coherence length of the recorded spectrum, which is determined by the light source spectrum and the angular scan range of the grating. When the scan range is chosen large enough (e.g., 500–700 nm), the entire LED spectrum is recorded. For this case, we have measured an axial resolution of 2 μm. The setup enables an

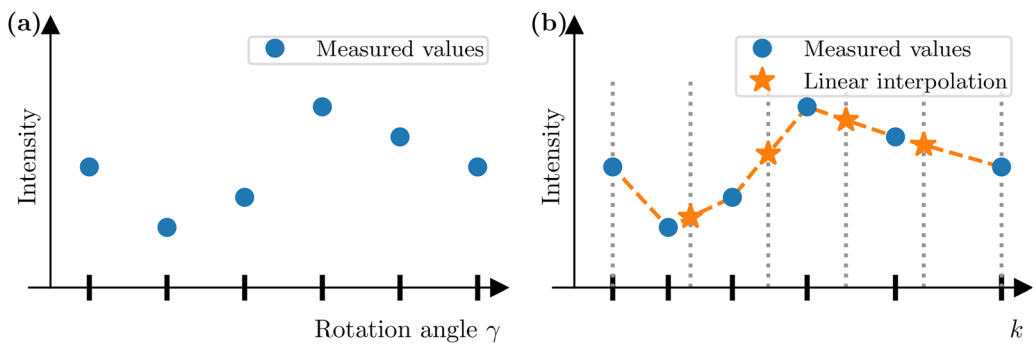

Fig. 4. (Color online) (a) Data acquisition: For each camera pixel, the intensities for different rotation angles γ are collected in equidistant steps. (b) Data processing for each pixel: Angles γ are converted to wave numbers k, using Eq. (8), yielding the modulated spectrum. The intensities are then linearly interpolated on an equidistant grid, so that the data can be Fourier transformed.

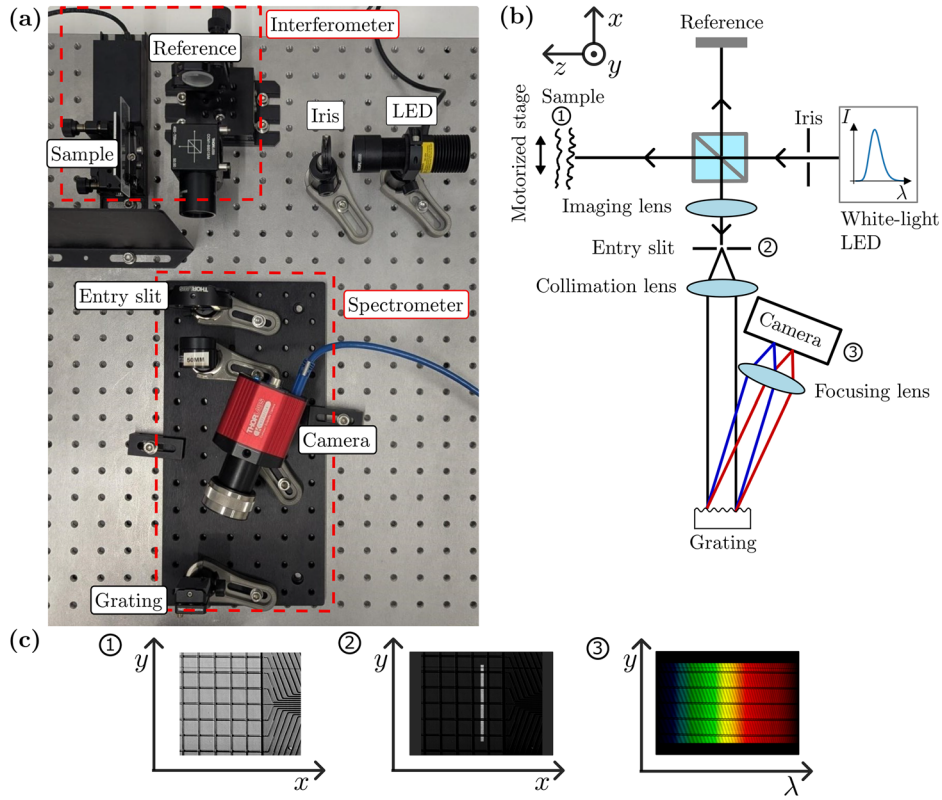

Fig. 5. (Color online) (a) Photograph of the spectral-domain setup. (b) Schematic of the beam path of the spectral-domain setup. A white-light LED illuminates the interferometer. The interference between light coming from each point of the sample (1) and the reference mirror results in a modulated spectrum, which is acquired by a spectrometer. The imaging lens projects an image of the sample onto the entry slit (2). Inside the spectrometer, the light is collimated and then incident upon a grating at normal incidence. The focusing lens in front of the camera forms an image of the entry slit, and consequently of one line of the sample, on the camera sensor (3) for each wavelength component. The grating separates the wavelength components along the horizontal direction of the camera due to diffraction. Thus, the spectrum for each point along the line of the sample is recorded within a single camera image. The depth information of the line is obtained via a Fourier transform of the spectrum, yielding a cross-sectional image of the sample. To generate a 3D scan, the motorized stage moves the sample perpendicular to the long axis of the slit. (c) Illustrations of the imaging at different points. (1) Sample that is imaged. (2) Image of the sample on the entry slit. Only light from one line of the sample enters the spectrometer. (3) Light incident on the camera. For each wavelength component, an image of the entry slit, and consequently of one line of the sample, is formed. Due to diffraction, different wavelengths are incident on different horizontal positions of the camera.

instructive experiment exploring the impact of the recorded spectrum. By reducing the angular scan range, the spectral width is reduced, which worsens the axial resolution. The reduced angular scan range also introduces sharp edges in the recorded spectrum, which lead to side lobes in the result after Fourier transformation.

The signal roll-off at larger measurement depths [Eq. (6)] is primarily determined by the linewidth of the light exiting the monochromator, provided that the wavelength sampling is fine enough. The sampling steps can be chosen freely by adjusting the ratio between exposure time and angular velocity. We typically measure at an average sampling step size of 0.2 nm. To quantify the signal roll-off for an entry slit width of 100 μm, we have measured the signal strength in dependence of the measurement depth for a single reflector in the sample arm. The signal halves at a measurement depth of 160 μm, which corresponds to a coherence length of 320 μm. Using Eq. (6), we can thus estimate a linewidth of $\delta\lambda = 0.5$ nm for the light exiting the monochromator. The setup can also be used to investigate the aforementioned relationship between the linewidth of the swept-source and the resulting signal. By increasing the slit width, the linewidth of the light exiting the monochromator becomes larger, and thus the coherence length is reduced, which results in less signal at larger depths, as shown in Fig. 6.

A 3D measurement takes about two minutes.

V. SETUP AND MEASUREMENT—SPECTRAL-DOMAIN OCT

In the following, we describe how our educational setup collects the spectral information to gain full 3D information of the sample.

A. Experimental realization

In standard spectral-domain OCT, a 3D measurement is typically obtained by focusing light onto a single point on the sample, collecting the returned light, and scanning the spot over an area, to acquire data point by point. In research or clinical systems, the acquisition process is optimized for speed so that a cross-sectional image of the sample (B-scan) appears in real time. While effective for imaging, this rapid scanning makes it difficult for students to observe how the data are gathered and processed, and the required high-speed scanners add significant cost. For our educational setup, we choose a more accessible and demonstrative approach. We use a self-built spectrometer that uses a 2D camera to record spectral information along one sensor axis (horizontal direction). The other axis records data from different lateral positions along a single line of the sample, with a separate modulated spectrum captured for each

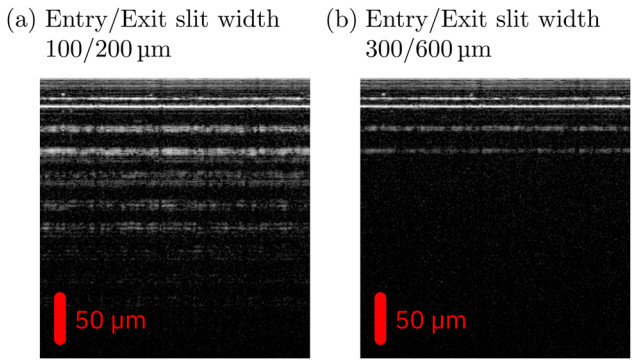

Fig. 6. (Color online) OCT cross-sectional views (B-scans) of several layers of adhesive tape, acquired with narrow and wide entry/exit slit widths (a) 100/200 μm and (b) 300/600 μm, respectively. Both images are displayed on a logarithmic brightness scale with identical brightness and contrast adjustments. The tape is composed of a PET backing film and an acrylic adhesive. The deeper interfaces appear broadened due to birefringence in the PET film. Increasing the slit width broadens the source linewidth, leading to stronger signal roll-off [Eq. (6)], and a reduced effective measurement depth.

position. This means each camera frame contains the depth information needed to reconstruct a complete B-scan in a single exposure. A 3D OCT image can then be assembled by moving the sample at constant velocity along the x-direction and recording successive frames. The setup is shown in a photo and sketch in Fig. 5.

The same white-light LED as in the swept-source setup illuminates the interferometer directly. A longpass filter is used to make the spectrum more closely resemble a Gaussian, to produce a clean OCT result [see Figs. 7(a) and 7(c)]. A lens at the output of the interferometer images the sample onto the entry slit of the spectrometer. Thereby, the entry slit not only serves as a typical spectrometer slit, but also as a spatial filter. The slit limits the spatial extent of the area on the sample from where the light is collected. In the spectrometer, a 50 mm achromatic lens behind the entry slit collimates the light. The collimated light hits a 600 lines/mm reflective grating at normal incidence. The horizontally dispersed light is collected by a 45 mm achromatic lens, which produces a sharp image of the entry slit on the camera sensor for each wavelength component. The placement of the camera unit can be challenging for students, as both its position and angle must be correct. Proper placement is achieved when the dispersed light passes through the center of the 45 mm lens and is imaged at the center of the camera sensor. To simplify this process, the camera height should be fixed first, and students should be provided with an approximate final position. We use the same 2D camera as in the swept-source setup to save cost. Each horizontal line of the camera image provides spectral information from a point on the entry slit and, thereby, a point on the sample. This allows a cross-sectional view of the sample (B-scan) to be constructed from one camera image. For a 3D scan, the sample is moved perpendicular to the optical axis by a motorized stage, while the camera acquires a sequence of images.

B. Calibration and alignment

After setting up the spectrometer, it must be calibrated, meaning that each horizontal pixel is assigned a wavelength value. In our testing, using bandpass filters at 500, 560, 600, 633, and 694 nm (all with 10 nm FWHM, except 1 nm FWHM for 633 nm filter) in combination with a quadratic fit yielded a reliable calibration.

When the sample is changed, two adjustments are necessary:

(1) The distance between the entry slit and the imaging lens must be set so that a sharp image is formed at the slit position.
(2) The Michelson interferometer must be realigned.

In the measurement configuration described in Sec. V A, these steps are not straightforward. Because of this, we have designed the following procedure to minimize effort when changing samples during a lab session:

(1) Positioning the entry slit: The slit must be located in the plane where the imaging lens forms an image of the sample. The spectrometer is set up on a separate breadboard so that the distance between imaging lens and entry slit can be adjusted. We utilize the fact that a sharp image in the plane of the entry slit translates to a sharp image on the camera sensor, when dispersion by the grating is negligible. To reduce dispersion, a very narrow bandpass filter (e.g., 1 nm FWHM, 633 nm laser line filter) is inserted in the beam path. The entry slit is removed (only the slit, not the holder), and the entire spectrometer breadboard is moved until a sharp image of the sample is visible on the camera sensor. The breadboard is then fixed in place with clamps.

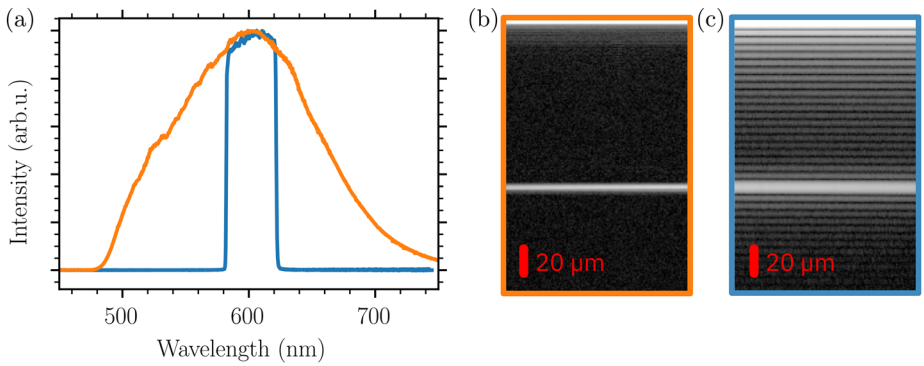

Fig. 7. (Color online) Effect of the spectral shape and spectral width on the OCT result. (a) Spectrum of the LED with a 495 nm longpass filter (orange) and the spectrum after passing through a flat top filter with a spectral width of 40 nm (blue). (b) Logarithmic OCT cross-sectional view (B-scan) of a sample with a single interface without the flat top filter. Because of the Gaussian-like spectrum, the interface appears as a single line in the result. (c) Logarithmic OCT cross-sectional view (B-scan) with the flat top filter. Due to the smaller spectral width when using the flat top filter, the line corresponding to the single interface appears broadened. Moreover, side lobes of both the DC term and the cross-correlation are visible as additional lines in (c), due to the shape of the spectrum.

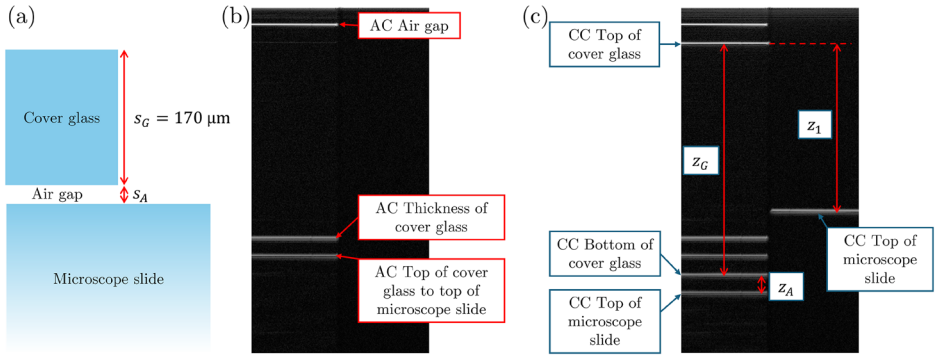

Fig. 8. (Color online) Refractive index measurement. a) A cover glass of thickness $s_G = 170\,\mu$m is placed on a microscope slide. There is a small air gap of thickness s_A in between (typically on the order of 10 μm). Panels (b) and (c) display spectral-domain OCT cross-sectional views (B-scans). Both images are displayed on a logarithmic brightness scale with identical brightness and contrast adjustments. (b) With the reference arm blocked, only auto-correlation (AC) lines are visible. (c) With the reference arm unblocked, both auto-correlation (AC) and cross-correlation (CC) lines are visible. To determine the refractive index n, three quantities are needed: optical thickness of the glass $z_G = ns_G$, optical thickness of the air gap $z_A = n_{\text{Air}}s_A \approx s_A$, and the combined thickness of glass and air gap $z_1 = n_{\text{Air}}(s_G + s_A) \approx s_G + s_A$.

(2) Aligning the Michelson interferometer: First, the position of the reference mirror is adjusted with the manual stage until interference fringes are visible on the camera sensor. Then, the angle of the sample relative to the reference plane is minimized. This is done by maximizing the size of the interference pattern, by iteratively adjusting the kinematic holder of the sample and readjusting the manual stage of the reference mirror to keep the interference pattern visible.

Once alignment is complete, the slit is reinstalled, the 1 nm filter is removed, and the setup is ready for measurement.

C. Data acquisition and processing

As described in Sec. V A, one camera image yields the spectral information for one transverse line of the sample. To analyze an image, the intensity information along the horizontal axis of the camera is assigned wave number values according to the spectrometer calibration. Since the pixels of the spectrometer camera are not equidistant in wave number, a similar interpolation as in the swept-source case (Fig. 4) is performed. After that, the data can be Fourier transformed.

Because every camera image captures the cross-sectional depth information along a transverse line of the sample (B-scan), the depth information can be viewed in real time. On a sufficiently fast computer, the interpolation and fast Fourier transform can be performed quickly enough that the cross-sectional view (B-scan) can be observed with a refresh rate of 50 Hz, thus demonstrating one major advantage that OCT has over other imaging modalities, e.g., confocal microscopy. This is also an advantage compared to our swept-source implementation, where the entire 3D measurement is needed to perform the interpolation and Fourier transformation. Here, the 3D measurement is optional. To gather full 3D data, the sample has to be moved perpendicular to the incident light. One practical aspect for the 3D measurement is the choice of the linear stage's scan speed. Ideally, the physical size of a pixel is the same in both directions of the sample surface. However, the vertical direction is determined by the imaging and camera pixel size, while the horizontal dimension is given by the frame rate of the camera and the stage speed. To gain knowledge about the physical extent of the camera image, we calibrate once with a USAF calibration target. That way, we know the physical extent of a pixel in the vertical direction and can choose the stage speed accordingly for the horizontal direction.

In a typical lab course setting, students should be guided through the procedures outlined in this section. Students can calibrate the setup for 3D measurements themselves.

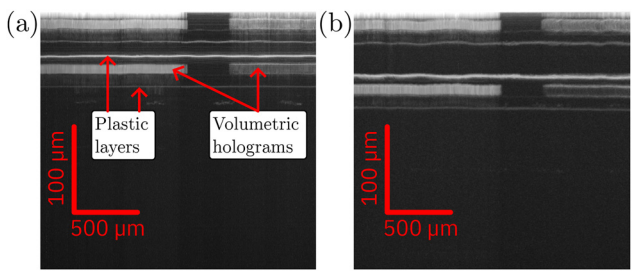

Fig. 9. (Color online) Logarithmic cross-sectional view (maximum intensity projection) for an identification card with embedded security holograms. (a) Acquired with the swept-source setup. (b) Acquired with the spectral-domain setup. The axial position of the sample relative to the reference plane differs from (a), which is why the cross-correlation signals appear at a different depth.

D. Performance

The lateral resolution was measured using a 1951 USAF target. We could resolve the lines of group 5 element 6, corresponding to a lateral resolution of 18 μm.

The axial resolution is equal to the coherence length of the recorded spectrum, which is determined by the light source spectrum and the wavelength range on the camera. We have designed the optical setup such that a majority of the LED spectrum is recorded (approximately 500–700 nm). We have measured an axial resolution of 2 μm.

The signal roll-off at larger measurement depths [Eq. (6)] is determined by the linewidth of the light that is measured by each pixel, i.e., the spectral resolution of the spectrometer. From a measurement of the sodium D-lines, we estimate the spectrometer resolution to be about $\delta\lambda = 0.5$ nm. Such a spectral resolution results in a coherence length of 320 μm [Eq. (3)] for the light measured by each pixel. This results in a halving of the signal-to-noise at an optical depth of 160 μm [Eq. (6)], which we have confirmed experimentally by measuring the signal strength's dependence on the measurement depth for a single reflector in the sample arm.

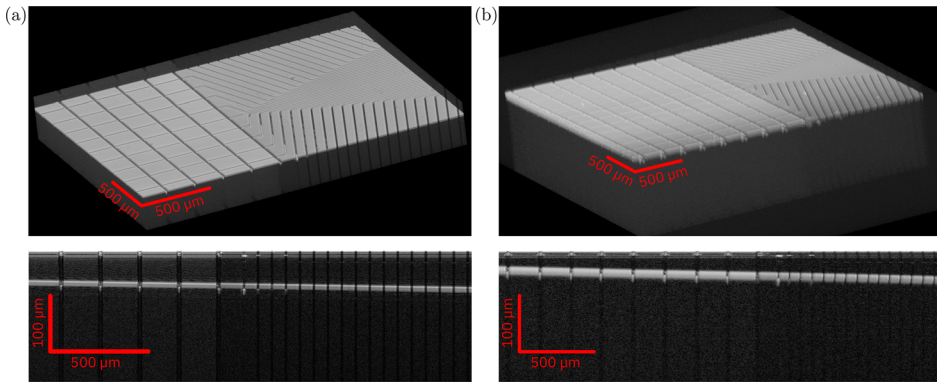

Fig. 10. (Color online) Measurement results for an OLED display. All images are displayed on a logarithmic brightness scale, and brightness and contrast have been adjusted. (a) Acquired with the swept-source setup. (b) Acquired with the spectral-domain setup. Top: 3D view of the chip plane. Bottom: cross-sectional view (B-scan).

A 3D measurement takes about 15 s.

VI. MEASUREMENTS

Here, we show some examples of measurements that can be performed with the two setups in an undergraduate laboratory. First, we show two measurements that illustrate how changing the system's properties influence the OCT result. Then, we show how the setups can be used to measure the refractive index of a glass plate. Finally, two sample measurements are shown.

A. Influence of the swept-source linewidth on signal roll-off

In the swept-source setup, the slit widths can easily be changed. Increasing the slit width broadens the source linewidth, which shortens the coherence length and leads to a faster signal roll-off [Eq. (6)]. As a result, the effective measurement depth is reduced. This is shown in Fig. 6 with several layers of adhesive tape as a sample. Students can clearly see that for larger slit widths, fewer layers are visible at greater depths. This hands-on experiment connects the abstract concept of coherence length with its concrete impact on the OCT imaging depth. The effect observed here can also be put into a more general measurement context: Any high-frequency signal measured with a bandwidth-limited device will exhibit decay in its Fourier-domain representation due to the filtering effect of the finite bandwidth.

We note that changing the slit width of the spectral-domain spectrometer is possible, but is more involved and gives a similar result.

B. Influence of the light source spectrum on OCT result

In both setups, spectral filters can be used to alter the spectrum of the light source. Because each peak along an OCT depth profile (A-scan) is given by the Fourier transform of the spectrum, changes to both the spectral width and the spectral shape will affect axial resolution and image artifacts.[13] To demonstrate the influence of the spectrum on the OCT result, a flat top filter with a spectral width of 40 nm is inserted. The filter should be inserted at a location where the beam is collimated and must not be placed in the interferometer arms. The impact of this filter on the spectrum and the OCT result is shown in Fig. 7, with the sample consisting of a single interface. Using the flat top filter gives an OCT result with worse axial resolution (Eq. 3 is not directly applicable, but shows the relationship between spectral width and axial resolution) and distinct side lobes, which fit the sinc function that is expected from the Fourier transform of a rectangular function. This experiment provides students with a hands-on demonstration of how source bandwidth governs axial resolution.

C. Measurement of the refractive index

Since OCT measures the optical path length, it can be used to determine refractive indices.[14] Here, we determine the refractive index of a 170 μm thick cover glass placed on top of a microscope slide [Fig. 8(a)]. This typically leaves an air gap on the order of 10 μm between the cover glass and the slide. Figure 8 shows the OCT result, and the assignment of the lines to auto- and cross-correlation. The auto-correlation lines correspond to distances between interfaces within the sample, while the cross-correlation lines represent the distances between each sample interface and the reference plane. Blocking the reference arm causes the cross-correlation lines to disappear, providing an easy experimental method to distinguish them from the auto-correlation lines [see Fig. 8(b)].

The group refractive index n is approximated by

$$n \approx \frac{z_G}{z_1 - z_A}, \tag{9}$$

where z_G, z_1, and z_A are optical lengths, which are defined in Fig. 8. This approach is adapted from earlier work,[14] with modifications to improve accuracy in the presence of an air gap between the sample and microscope slide.

The measurement result $n = 1.54 \pm 0.02$ is close to the published value of 1.55 for SCHOTT D263® glass[15] at 600 nm. The stated uncertainty is estimated from the readout error of the interface depths.

D. Imaging

With an identification card as a sample, the volumetric holograms in between two plastic layers can be visualized. Figure 9 shows cross-sectional images of an identification card for both setups. The relative distance between the top surface and the reference plane was adjusted such that the auto-correlation and cross-correlation are clearly distinguished.

For the OLED display in Fig. 10, the pixels and the electrical connections can be imaged in 3D with both setups. The OLED measurement shows how OCT applies to real-world devices students encounter daily. OCT is, in fact, used by display manufacturers to ensure production quality.

VII. CONCLUSION

We have presented two educational setups for students to explore Fourier-domain OCT. These two setups allow hands-on investigation of the two most commonly used OCT methodologies: spectral-domain and swept-source OCT. Each setup demonstrates the underlying principles of the method in an educational way and yields a three-dimensional sample measurement. Although the setups presented here deliver good results, their main strength lies in their focus on the methodology. With a simple and open experimental realization, rather than a black box, we pave the way for a better understanding of OCT, in particular, and coherence, in general.

SUPPLEMENTARY MATERIAL

Please click on this link to access the supplementary material, which includes notes on light source selection and a list of the main components used to build up the two setups. Print readers can see the supplementary material at https://doi.org/10.60893/figshare.ajp.c.8245807.

AUTHOR DECLARATIONS

Conflict of Interest

The authors have no conflicts to disclose.

Author Contributions

K.P. developed the swept-source OCT setup with guidance from J.K., A.B. and C.R., K.U., and J.K. developed the spectral-domain OCT setup. K.U. and M.A. performed the measurements. M.A. drafted the manuscript, and all authors reviewed and approved the final version.

[a]ORCID: 0009-0009-6962-0922.
[b]ORCID: 0000-0003-1366-671X.
[c]ORCID: 0000-0002-6581-8335.
[d]Electronic mail: antje.bergmann@kit.edu, ORCID: 0000-0002-5822-8759.
[e]ORCID: 0000-0002-5868-0526.
[f]Electronic mail: JKuechenmeister@thorlabs.com, ORCID: 0009-0002-2006-5453.

[1]M. Adhi and J. S. Duker, "Optical coherence tomography—Current and future applications," Curr. Opin. Ophthalmol. **24**(3), 213–221 (2013).
[2]T. Yonetsu and I.-K. Jang, "Cardiac optical coherence tomography," JACC **4**(2), 89–107 (2024).
[3]N. S. Samel and H. Mashimo, "Application of OCT in the gastrointestinal tract," Appl. Sci. **9**(15), 2991 (2019).
[4]B. R. Davidson and J. K. Barton, "Application of optical coherence tomography to automated contact lens metrology," J. Biomed. Opt. **15**(1), 016009 (2010).
[5]M. Wagner, D. Taherzadeh, C. Haisch, and H. Horn, "Investigation of the mesoscale structure and volumetric features of biofilms using optical coherence tomography," Biotechnol. Bioeng. **107**(5), 844–853 (2010).
[6]T. Callewaert, J. Guo, G. Harteveld, A. Vandivere, E. Eisemann, J. Dik, and J. Kalkman, "Multi-scale optical coherence tomography imaging and visualization of Vermeer's Girl with a Pearl Earring," Opt. Express **28**(18), 26239–26256 (2020).
[7]K. Pieper, G. Latour, J. Küchenmeister, A. Bergmann, R. Dengler, and C. Rockstuhl, "Full-field optical coherence tomography—An educational setup for an undergraduate lab," Am. J. Phys. **88**(12), 1132–1139 (2020).
[8]S. Kim, M. Crose, W. J. Eldridge, B. Cox, W. J. Brown, and A. Wax, "Design and implementation of a low-cost, portable OCT system," Biomed. Opt. Express **9**(3), 1232–1243 (2018).
[9]R. S. Jonnal, O. P. Kocaoglu, R. J. Zawadzki, Z. Liu, D. T. Miller, and J. S. Werner, Invest. Ophthalmol. Visual Sci. **57**, OCT51–OCT68 (2016).
[10]A. Dubois, *Handbook of Full-Field Optical Coherence Microscopy: Technology and Application* (Jenny Stanford Publishing, 2016).
[11]W. Drexler and J. G. Fujimoto, *Optical Coherence Tomography—Technology and Application* (Springer International Publishing, 2015).
[12]J. A. Izatt, M. A. Choma, and A. Dhalla, in *Optical Coherence Tomography—Technology and Application*, edited by W. Drexler and J. G. Fujimoto (Springer International Publishing, 2015), pp. 65–94.
[13]C. Akcay, P. Parrein, and J. P. Rolland, "Estimation of longitudinal resolution in optical coherence imaging," Appl. Opt. **41**(25), 5256 (2002).
[14]G. J. Tearney, M. E. Brezinski, J. F. Southern, B. E. Bouma, M. R. Hee, and J. G. Fujimoto, "Determination of the refractive index of highly scattering human tissue by optical coherence tomography," Opt. Lett. **20**(21), 2258 (1995).
[15]Schott, "Optical glass—overview glass types (zemax format)," <https://www.schott.com/en-us/products/optical-glass-p1000267/downloads> (2025).